Tensile properties and interfacial shear strength of recycled fibers from wind turbine waste

Amirmohammad Rahimizadeh [a], Mazin Tahir [a], Kazem Fayazbakhsh [b,*], Larry Lessard [a]

[a] *Department of Mechanical Engineering, McGill University, Montreal, QC H3A0C3, Canada;*
[b] *Department of Aerospace Engineering, Ryerson University, Toronto, Ontario M5B2K3, Canada;*
kazem@ryerson.ca
**Corresponding author: kazem@ryerson.ca; Tel: (+1) 416-979-5000 ext. 6414; fax: (+1) 416-979-5056*

Abstract

The rapid growth of composites combined with imminent recycling legislation have increased the interest in reusing and recycling of composite waste. Tensile strength and interfacial shear strength (IFSS) of recycled fibers are critical factors contributing to the final properties of recycled products. Here, we focus on the tensile properties of recycled glass fibers from scrap wind turbine blades and their interface strength with polylactic acid (PLA). The single fiber tensile and pull-out tests are used to characterize the fibers recovered through mechanical and thermal processes. It is shown that while pyrolysis can significantly degrade the recovered fibers, ground fibers with a gage length of 20 mm feature characteristic strength comparable to that of virgin fibers. The effect of the fibers surface coating on the IFSS are investigated, with results showing an interface between ground fibers and PLA that is 14% and 26% stronger than pyrolyzed and virgin fibers, respectively.

Keywords: A. Wind turbine blade, A. Polylactic acid, D. Single fiber tensile test, D. Single fiber pull-out test.

Composites Part A Journal

https://doi.org/10.1016/j.compositesa.2020.105786

1. Introduction

The load carrying capacity of composites is mainly governed by the mechanical properties of the reinforcement material and the interfacial bonding strength [1]. While the reinforcement material is mainly responsible for resisting against the applied loads, the fiber-matrix interface plays a key role in transferring the load to the fibers. Interfacial bonding is a metric that is determinant to the composite strength and stiffness by increasing the load transferring capacity of the composites. Even though expensive and complex, optimizing the fiber-matrix interface through fiber treatment technologies has shown to be beneficial in enhancing the interfacial bonding [2]. For instance, glass fibers are typically covered with functional agents through the sizing technology [3]. Despite forming a protective layer, the sizing agents can contribute to the binding of the matrix and fibers by providing the opportunity for chemical interactions at microstructural scales [3].

Recent overwhelming use of composites, which raises environmental sustainability concerns, has motivated the reuse of fiber reinforcements from composite waste into new material systems. Wind turbine rotor blades will soon represent one of the major composite waste-generating sources as a tremendous number of turbines are coming to their end-of-life and will be soon decommissioned all around the world [4]. Turbine blades are mainly composed of glass fibers and epoxy or vinyl ester polymers [4]. Thermal, chemical, and mechanical processes are widely proposed to reclaim fiber reinforcements from thermoset scrap blades [5]. However, current recycling routes for scrap rotor blades have only been partially successful because the recycling of rotor blades comes at the expense of fiber strength reduction and interface degradation [6]. The thermal and chemical processes generally result in the inevitable reduction in the fiber properties, which deteriorates the viability and effectiveness of recycling [7, 8]. For instance, Cunliffe et al. [9] have documented a substantial reduction of 40-50 % in the mean tensile strength of E-glass fibers recovered from

polyester sheet molding compound (SMC) using the pyrolysis technique. These techniques also require a high amount of waste and a very large plant, which translates into a relatively large investment to motivate such techniques. Another drawback limiting the extensive use of these recycling processes is the degradation of fiber sizing, which in turn necessitates an additional post-treatment process to improve their processability, as well as the interfacial bonding between the recycled fibers and the new resin matrix [10]. The post-treatment process on thermally recycled fibers is typically challenging since they are generally brittle and break during the compounding process generating numerous new untreated surfaces. The sizing removal can also introduce adverse effects on the mechanical performance of the fibers by exposing surface defects and lowering the fiber strength [11]. In an experimental study, Nzioka et al. [8] applied a chemical recycling scheme coupled with ultrasound cavitation to recover E-glass fibers from scrap composite parts. The surface analysis results showed a lower quality non-smooth surface topology for the recovered fibers. However, coating the fibers surface with 1 wt% APS silane agents helped to improve the surface topography.

Unlike the thermal and chemical recycling techniques, mechanical grinding is a straight forward and economically feasible solution for recycling of composites. This technique offers a fast and efficient technique to decrease the size of waste and reclaim fibers with low aspect ratio [12]. The ground fibers differ from thermally or chemically recycled ones by not only preserving the surface sizing, but also the presence of matrix residue on the surface, a phenomenon which highly increases the fiber surface roughness. If used with an appropriate new resin, the presence of the matrix powder on the surface of fibers can allow for mechanical and chemical interactions, where the former results from surface roughness and the latter arises from molecular interactions. Nonetheless, long fibers cannot generally be preserved by mechanical recycling. As a result,

mechanically recycled fibers are typically used in composites with short fibers as reinforcement, such as the ones manufactured by bulk molding compound [13]. While the early studies on the mechanical recycling of composites have noticed the different morphology of the recycled fibers, they have mainly focused on the bulk properties of the composites made out of the recycled fibers and they fall short in precisely characterizing the recycled fibers [12].

The authors of this research work used mechanical grinding of wind turbine waste and recently introduced a composite 3D printing filament made of polylactic acid (PLA), a biodegradable thermoplastic used extensively in 3D printing and injection molding, and recycled glass fibers [14]. A systematic mechanical recycling scheme was proposed and applied to a set of scrap turbine blade pieces to reclaim short fibers from end-of-life rotor blades. Using ground E-glass fibers, structurally stiff filaments were manufactured and used to 3D print parts with superior structural properties. A subsequent study confirmed that the ground fibers retaining resin residue have higher structural properties when mixed with PLA compared with those made of virgin glass fibers with silane sizing and PLA [15]. In these early studies, mechanical testing of 3D printed coupons per ASTM D638-14 was performed, which provides only limited insight into the properties of recycled fibers. Recently, Cousins et al. [4] studied the mechanical properties of fibers recovered from thermoplastic wind turbine blades through a dissolution recycling process. In this study, rovings from the recovered fibers were prepared and tested. The results revealed a reduction of 12 % in the stiffness of the fibers, which was attributed to the possible fiber degradation during the recycling process. Furthermore, the feasibility of reusing ground thermoplastic blades in injection moulding was investigated. However, no micromechanical analysis on the tensile properties and interfacial strength of the ground fibers was carried out. More recently, a two-stage pyrolysis method was used to reclaim E-glass fibers from wind turbine blades [7]. In this study, the tensile

strength of the recovered fibers was only characterized and compared with virgin fibers. Consequently, further research work on precisely characterizing the recycled fibers from end-of-life wind turbine blades is crucial to identify proper applications for the use of them.

In this work, the mechanical properties of reclaimed glass fibers from end-of-life scrap turbine blades are characterized and their interfacial strength with PLA is measured. On the first front, the mechanical properties of single recycled fibers extracted thermally and mechanically from scrap blades are characterized for different gage lengths, namely 20, 40, and 60 mm. On the second front, the interfacial strength between the recycled fibers and PLA is assessed using single fiber pull-out test and compared with a baseline, virgin glass fibers and PLA. The test is performed over a wide range of embedded length ranging from 60 – 400 μm. Lastly, the mechanical and interfacial properties of the recycled fibers are used to calculate the critical fiber length required to design recycled composites with effective strength and stiffness.

2. Materials and methods

The thermal and mechanical recycling methods are used here to obtain glass fibers from end-of-life wind turbine blades. The mechanical recycling steps are illustrated in Figure 1. As depicted, the scrap parts from wind turbine blades are first cut into small 20 cm × 20 cm pieces using a bandsaw. The pieces are then ground using a hammer mill grinder (ECO-WOLF, INC.). To obtain fiber bundles with an appropriate length for single fiber tests, a screen classifier with a hole size of 19 mm is used.

The thermal recycling of the scrap blades is carried out after an initial granulation process, as described above. Following the grinding process, 100 g of the recyclate materials is placed in the pyrolysis furnace (F200 PYRADIA, Quebec, Canada) at 550 °C and retained for a total duration of 45 min. The pyrolysis process is performed in the presence of nitrogen followed by an oxidative

stage at 550 °C for 10 min to remove the ash content left on the surface of the recovered fibers, as shown in Figure 1D. Subsequently, individual fibers from fiber bundles of both mechanically and thermally recycled compounds are carefully separated and used for single fiber tensile and pull-out tests. For convenience, mechanically recycled fibers before pyrolysis and thermally recycled fibers after pyrolysis are hereafter referred to as ground fibers and pyrolyzed fibers, respectively.

Wind turbine blades are generally made of epoxy and E-glass fibers with a diameter ranging between 3.8 and 20 μm [16]. The average diameter of the recovered fibers in the present study is predicted by measuring the diameter of at least 100 fibers from the recyclate compound using an optical microscope. The average diameter is then used to calculate the cross-sectional area of single fibers. To capture the surface topology of the recycled fibers, scanning electron microscopy (Hitachi UHR Cold-Emission FE-SEM SU8000) is conducted on the recycled fibers and virgin E-glass fibers, a baseline fiber with sized surface finish.

2.1 Single fiber tensile test

The mechanical properties of the recycled fibers are characterized through the single fiber tensile test. Single fibers are carefully extracted from ground and pyrolyzed fiber bundles at random and glued onto card tabs with a specific gage length (Figure 2). To separate off single ground fibers, a ground bundle is first cut into small pieces and then single fibers are separated using a tweezer. The tabs are then gripped by a universal testing machine (Instron Model 3342) equipped with a load cell of 10 N. Enormous care is taken to ensure that the axis of the fibers is aligned with the axis of the cross-head. The test is conducted at a displacement rate of 0.1 mm/min. To study the effect of the gage length on the tensile properties of single fibers, three sets of samples with gage length of 20, 40, and 60 mm are prepared. As suggested by previous works in the literature, a total of at least 10 samples for each gage length are tested [17, 18].

2.2 Single fiber pull-out test

Several micromechanical approaches, including the single fiber pull-out test, the microdroplet test, the push-out test, and the single fiber fragmentation test are proposed in the literature to characterize interfacial shear strength (IFSS) [19, 20]. The single fiber pull-out test has been broadly used for thermoplastic composites, which feature weaker adhesion [21]. According to this method, a single fiber is pulled out of a matrix droplet or block with a specific embedded length. To ensure an interface failure during the test, the length of the embedded fiber has to be less than half of the critical length of the fiber, as explained in [1]:

$$L_e < \frac{\sigma_f d}{4\tau} \tag{1}$$

where σ_f, d and τ are, respectively, the tensile strength of the fiber, diameter of the fiber, and the interfacial strength. Controlling the embedded fiber length, especially for thermoplastic polymers, plays an important role in the success and accuracy of this test. Although the single fiber pull-out method has been widely used to determine the apparent interface bonding strength, the reliability and accuracy of IFSS values obtained via this method and other techniques should be regarded with some caution due to several limitations. For instance, in the calculation of IFSS, a constant stress distribution along the fiber interface is assumed, a simplification that is shown to be invalid [22]. In addition, the interfacial failure is associated with some intact regions, which contribute to the peak load through frictional forces [21]. Herein, the interfacial analysis between reclaimed glass fibers from scrap blades and PLA (Ingeo 4043D, Natureworks LLC, Blair, Nebraska) is undertaken using the single fiber pull-out test to carry out a comparison study between the apparent IFSS in three different composite systems including ground fibers/PLA, pyrolyzed fibers/PLA and a baseline, virgin E-glass fibers/PLA.

2.2.1 Preparation of samples for single fiber pull-out test

Figure 3 illustrates the methodology used to prepare samples for measuring the apparent interfacial strength between either ground or pyrolyzed glass fibers, and PLA using the single fiber pull-out test. Individual fibers are carefully separated and glued onto card tabs. A soldering iron is used to melt PLA pellets and obtain PLA stripes with different width, representing the embedded length. The PLA stripes are then placed on microscope slides, which allow for an accurate measurement of the embedded length. Using a soldering iron, the stripes are first slightly heated to firmly adhere to the slides. Then, the other end of the fibers is placed on the PLA stripes and heated again to slightly embed within PLA. At the end, a total of at least 15 samples are prepared and transferred to an oven with a temperature of 200 °C and maintained for 4 minutes. This heating program will ensure complete melting of the PLA resulting in fibers that are properly embedded within the PLA.

Once the samples are cooled down to ambient temperature, the exact embedded length of the fibers is captured using a Nikon visual microscope. The sample are then vertically placed in the tensile test machine and tested using a 0.1 mm/min displacement rate until interfacial failure. One major issue associated with single fiber pull-out test is the formation of a meniscus around the fiber surface. The meniscus does not contribute to the interfacial strength and undergoes a cohesive rupture prior to adhesive debonding at the interface [23]. To minimize the effect of the meniscus in our calculation, each specimen is carefully inspected after the test to accurately capture the trace of the fiber and remeasure the true embedded length (Figure 4). Furthermore, this inspection will ensure that unacceptable failure modes such as debonding of the PLA stripe from the glass slide, have not occurred.

As shown in Figure 5, the distribution of the maximum load versus the embedded length for all the samples are then plotted and used to predict the apparent IFSS. Given the non-uniform stress

distribution along the fiber interface, the slope of a regression line passing through the data points is used to calculate the interfacial strength, as suggested in [24]:

$$\tau_{d1} = \frac{s}{\pi d} \tag{2}$$

where s and d represent the slope of the regression line and average fiber diameter, respectively. Samples that failed due to PLA stripe debonding or fiber fracture are not considered in the IFSS results. To examine the effect of fiber surface sizing, samples with virgin glass fibers are prepared and tested using the procedure described above. The virgin glass fibers are coated with silane sizing, the most commonly used sizing agent to improve their compatibility with polymers.

3. Results and discussion

This section summarizes two sets of results describing the tensile properties of the recovered and virgin fibers, as well as their surface morphology and interfacial bonding with PLA.

3.1. Single fibre tensile test

Figure 6 shows the diameter distribution of the recycled glass fibers prior to the pyrolysis process. As seen, the recyclate compound consists of fibers featuring different diameters ranging between 12-21 μm. An average fiber diameter of approximately 17 μm was obtained and used for the strength and IFSS calculations.

SEM micrographs from the recycled and virgin fibers are shown in Figure 7. These images revealed that the ground fibers feature a higher surface roughness due to the presence of epoxy particles fractured off the adjacent fibers during the grinding process. On the other hand, SEM images from both pyrolyzed and virgin glass fibers showed a smoother surface when compared to the ground fibers. However, some regions with uneven impurities can still be identified on the surface of both fibers, e.g. virgin and pyrolyzed.

While SEM images clearly showed the rougher surface of the ground fibers compared to the virgin baseline fibers, atomic force microscopy (AFM) was used to accurately capture the surface topology of the recycled fibers and compare to that of virgin fibers. A JPL AFM machine (JPK Nano-wizard@3 BioScience, Berlin, Germany) was used for surface imaging. Fibers were gently placed and glued to microscope glass slides, such that no movement occurred during the imaging process. The maximum lateral scan was focused on regions with area of 5 μm × 5 μm, and AFM images were obtained at a resolution of 512 × 512 pixels. The surface imaging was completed for 3 regions for a total of 3 samples for each fiber. Figure 8 shows representative AFM height images from the surface of the ground, pyrolyzed and virgin fibers. As observed, the surface of the ground fibers is covered with numerous lumps of different sizes caused by residue epoxy particles. The AFM images from the pyrolyzed fibers manifested a surface topology with a rug-like structure, which could be attributed to the removal of the silane coating during the pyrolysis. Further, some regions with large protrusions were detected on the surface of the pyrolyzed fibers. These lumps that were irregularly distributed throughout the surface of the fibers were attributed to the incompletely decomposed polymer resin left on the fibers surface. In contrast, the virgin fibers featured a homogenous and smooth surface topology compared to the pyrolyzed fibers. However, random heterogeneities were also detected at some regions, which could be attributed to the sizing tearing during the extraction process. To capture the roughness of the fibers, JPK data processing software was used to obtain the surface height diagrams along the fiber longitudinal axis. These diagrams were obtained at three different locations and then utilized to measure the average roughness (R_a), as well as the root mean square roughness (R_q). As shown in Table 1, the results demonstrated that the ground fibers feature a surface topography with an average roughness that is one order of magnitude larger than that of pyrolyzed and virgin fibers. In addition, the removal

of the silane coating, as well as the presence of undecomposed epoxy particles on the surface of the pyrolyzed fibers have contributed to their higher surface roughness compared with the virgin fibers.

Figure 9 displays the tensile properties of the ground, pyrolyzed and virgin fibers versus the gage length. The error bars show the standard deviation (SD) of multiple tests. It should be noted that a smaller number of ground fibers with a gage length of 60 mm were successfully separated and tested owing to the ease of fiber breakage with these longer fibers. Hence, the results for this gage length were only included for completeness.

The mean fiber tensile properties, i.e. strength, stiffness, and strain to failure, along with the SD values are summarized in Table 2. As expected, the fibers showed a brittle failure mode with an average strength decreasing with the increase in the gage length. The mechanical behaviour of fibers is mainly governed by the distribution of defects on their surface such that shorter fibers feature lower quantities of surface flaws. On the other hand, fibers with larger surface area incorporate a larger number of extrinsic surface defects, which increases the chance of microcrack formation. Hence, SD values can be mainly attributed to the variation of flaw distribution on the surface of fibers. As shown in Table 2, the average strength of the ground fibers reduced by 15 % with an increase in the gage length from 20 mm to 40 mm. As well, increasing the gage length from 20 mm to 60 mm led to a reduction of 30 % in the mean strength of the pyrolyzed fibers. In addition to strength, the ductility of the fibers with a gage length of 60 mm was remarkably lower than that of fibers with a gage length of 20 mm for both ground and pyrolyzed fibers. Compared with ground fibers, it is noticeable that the pyrolyzed fibers showed lower ultimate strength with values decreased by 50 % and 52 % for the 20 and 40 mm gage lengths, respectively. While removing the surface impurities, e.g. epoxy residue, is expected to improve the strength, this

reduction can be attributed to the degradation of E-glass fibers at high temperatures used in pyrolysis [25-27]. We also observed that pyrolyzed fibers are much more brittle compared to the ground fibers with failure strain reduced by 47 % and 56 % for the 20 and 40 mm gage lengths, respectively.

As a baseline, the tensile properties of the virgin fibers were characterized and summarized in Table 2. The average tensile properties reported in the literature align well with those herein measured [28]. As seen, a similar trend appeared in the mechanical properties of the virgin fibers, such that an increase in the gage length was associated with a reduction in the tensile strength and ductility. As expected, virgin fibers exhibited the highest tensile strength with an average value 20 % and 19 % higher than that of ground fibers with gage lengths of 20 mm and 40 mm, respectively. Compared with the pyrolyzed fibers, virgin fibers showed 60 %, 61 % and 65 % higher values in tensile strength for gage lengths of 20 mm, 40 mm and 60 mm, respectively.

As per the elastic modulus, pyrolyzed fibers showed higher stiffness compared with ground fibers with values improved by 9 % and 17 % for the 20 and 40 mm gage lengths, respectively. The disparity in the stiffness values can be attributed to the molecular network compaction that happens during the pyrolysis process resulting in an increase in the density of the fibers, thereby improving the stiffness [29]. Nevertheless, the mean stiffness of the ground fibers at different gage lengths was comparable with that of virgin fibers, indicating that no degradation in the stiffness of the fibers occurs after mechanical recycling. In contrast to strength, it is demonstrated in the literature that fibers with longer gage length tend to show higher modulus [30]. This behaviour is mainly due to the fact that increasing the gage length is associated with a higher rate of reduction in the ductility of fibers as compared with their ultimate strength. Despite some variations, we observed the same trend in the pyrolyzed and virgin fibers, where the mean stiffness value somewhat

increased by increasing the gage length. On the other hand, the ground fibers showed a larger variation in the stiffness results such that the mean stiffness value for different gage lengths remained at the same level.

As shown in Figure 10, the non-uniform distribution of the epoxy particles, as well as the surface damage caused by grinding lead to a more dispersed defect distribution on the surface of the ground fibers as compared to virgin and pyrolyzed fibers. The amount of resin residue on the surface of the ground fibers varies from one fiber to another, a variation that influences the tensile performance of the fibers. This irregular defect distribution results in variable surface topographies, particularly for fibers with short gage length. Depending upon the surface flaw distribution, on one hand, the presence of the epoxy residue could be beneficial to the performance of the ground fibers as the surface pitting are filled with epoxy, thus microcracks formed around these spots tend to propagate through the epoxy particles due to their weaker mechanical properties compared to glass fiber. On the other hand, the bulk epoxy protrusions could serve as surface defects by changing the local geometry of the fibers and generating stress concentration. In addition, the presence of epoxy could impact the surface deformation rate of the fibers, when subjected to axial loads. The varying distribution of the epoxy residue could be the major cause for the large variations in the tensile properties of the ground fibers with different gage lengths.

To represent the distribution of the strength data obtained for the recycled fibers, a two-parameter Weibull function is used as follows:

$$P_{\sigma_a} = 1 - exp[-(\frac{L}{L_o})(\frac{\sigma_a}{\sigma_o})^w] \quad (3)$$

where P_{σ_a} is the cumulative probability of fiber failure for a gage length of L and at a stress level lower than or equal to σ_a , and L_o is the reference length. σ_o and w denote the Weibull scale and

shape parameters, respectively. To find the Weibull parameters, the strength data for each gage length is sorted in an ascending order and a probability function is used to identify the probability of fiber failure for the *i*th strength point, as follows:

$$P_{\sigma_i} = \frac{i - a}{N - b} \tag{4}$$

where N represents the total number of strength data points. Also, a and b are statistical parameters with a value of 0.5 and 0, respectively [21]. To obtain the Weibull parameters, Eq. 3 is rearranged, and logarithm of both sides is taken to define the following relation:

$$\ln\left[-\ln\left(1 - P_{\sigma_a}\right)\right] = w ln(\sigma) - w ln(\sigma_o) \tag{5}$$

It should be noted that in Eq. 3, the scale parameter is defined as fiber strength at a gage length identical to the reference length. Figure 11, 12 and 13 show, respectively, a plot of $\ln\left[-\ln\left(1 - P_{\sigma_a}\right)\right]$ versus $ln(\sigma)$ for the ground, pyrolyzed and virgin fibers, where the slope and the y-intercept are used to determine the Weibull shape and scale parameters, respectively. Due to the low data points for the ground fibers with the gage length of 60 mm, the Weibull plot is not shown. As seen, a satisfactory agreement between the Weibull regression line and the tensile results is observed for all the fiber systems.

The Weibull shape (w) and scale parameter (σ_o) for the ground, pyrolyzed and virgin fibers are summarized in Table 3. As observed, the virgin fibers feature the largest scale and shape parameters, indicating the highest properties with the lowest scatter. In addition, the pyrolyzed fibers feature a larger shape parameter compared to the ground fibers, indicating a narrower distribution of the strength data. The difference in the strength distribution is in agreement with the results of previous works [31]. The large variation in the strength results of the ground fibers

arises from the random distribution of the epoxy particles, as well as the surface damage caused by grinding. Noticeably, the scale parameter for the ground fibers with a gage length of 20 mm shows that 63% of the ground fibers fractured with an average strength level of above 2190 MPa, a value that is comparable to that of virgin fibers with only 18 % difference. This observation highlights that due to the lower stiffness of epoxy as compared to glass fiber, the role of the resin residue in lowering the strength by generating stress concentration spots is not only negligible, but also critical to the retention of fiber strength by filling up the surface defects. In contrast, the pyrolyzed fibers exhibited lower characteristic strength compared to that reported in the literature [31]. This reduction could be attributed to the excessive damage caused to the fibers during the grinding process.

3.2. Single fiber pull-out test

The maximum load versus embedded length results from the pull-out test of the recycled fibers (ground and pyrolyzed) and the virgin glass fibers are plotted in Figure 14. A representative force-displacement curve for each fiber type is presented, as well. The force-displacement curves show a typical behaviour observed in pull-out tests, where the debonding process initiates immediately at peak load and following the interfacial failure, the load drops down to near zero. As shown in Figure 14A, continuing the test leads to a minor increase in the load, which corresponds to the frictional force developed at the interface.

Using the slope of the regression lines in Figure 14 and Eq. 2, the apparent IFSS value for the virgin, ground, and pyrolyzed fibers are calculated (Table 4). The results confirmed a stronger interfacial bonding between the ground fibers and PLA, featuring an IFSS higher than the pyrolyzed and virgin glass fibers by 14 % and 26 %, respectively. The larger IFSS for the ground fibers relative to virgin and pyrolyzed fibers stems from the epoxy matrix residues, which increase

the fibers surface roughness and allow for better molecular mechanical interactions and interlocking. In addition, epoxy molecules can chemically interact with PLA molecules through the development of hydrogen bonding, which could further improve the apparent IFFS around the ground fibers [32]. The results also showed that the pyrolyzed fibers feature a higher IFSS compared with virgin glass fibers, a result that correlates with the higher surface roughness of the pyrolyzed fibers. The larger IFSS around the pyrolyzed fibers also elucidates the negligible effect of the silane coating on the interfacial bonding. This observation matches well with previous investigations on the effect of silane coating on the properties of composites made of pyrolyzed fibers from wind turbine blades [33]. It is well demonstrated in the literature that sizing coating should be optimized for a specific fiber and resin matrix to improve the interfacial chemical bonding. Herein, the silane sizing present on the surface of virgin E-glass fibers was optimized for epoxy, thus it does not necessarily contribute to any chemical reactions at the interface with PLA.

One important factor determining the final properties of short fiber composite structures is the critical length of fiber reinforcements. To efficiently use the maximum fibers strength, the length of the fibers should be larger than the minimum required critical length. Further, it is shown in the literature that fibers shorter than critical length could serve as defects, lowering the strength of the composite relative to pure resin material [34]. The critical length of fibers can be predicted using the fibers strength and interfacial shear strength as:

$$l_c = \frac{\sigma_f d}{2\tau} \tag{6}$$

where σ_f, d and τ are the fiber strength, fiber diameter, and the interfacial shear strength, respectively. Considering the large variation observed in the recycled fibers strength, a lower and upper bound critical length can be predicted. Table 4 shows the values for the critical length of the

recycled fibers. These results can provide insight into the minimum required fiber length to achieve effective strengthening and stiffening using the recycled fibers. As can be seen, the ground fibers feature a wider range with a larger upper bound compared with pyrolyzed ones. This indicates that longer ground fibers should be utilized to obtain composites with efficient mechanical properties.

An extensive amount of literature has investigated the critical role of interface shear strength on the failure mechanism and final properties of composites [35, 36]. Previous works have shown that a strong fiber-matrix interface can enhance the fiber load carrying contribution in the composite, thus increasing the tensile properties of the composite [37]. With tensile properties comparable with virgin fibers, the capability of the ground fibers to form a strong adhesion with PLA enables the fabrication of effective composites out of short fibers extracted from end-of-life scrap blades. In a comparative study between short fiber composites made of ground fibers from end-of-life wind turbine blades and virgin fibers, the mechanical properties of recycled composites have been successfully characterized [15]. The ground and virgin short fibers used in this investigation shared identical dimensional properties, i.e. fiber length distribution and fiber diameter. As a result, the differences between the mechanical properties of the composites were exclusively ascribed to their micro-mechanical properties, namely fiber properties and interface strength. The results from this investigation demonstrated that the recycled composites made of ground fibers feature tensile strength and stiffness that are, respectively, 19% and 18 % higher than those of composites made from virgin fibers. This previous work therefore demonstrates the potential of mechanically recycled fibers from scrap wind turbine blades in manufacturing composites with effective properties.

Conclusion

In this work, we have focused on the tensile and interfacial characterization of recovered fibers from end-of-life wind turbine blades. The single fiber tensile and pull-out tests were employed to characterize the tensile properties of mechanically and thermally reclaimed fibers, as well as the interface strength between the recovered fibers and PLA. The results from the single fiber tensile test revealed that the tensile strength of the pyrolyzed fibers relative to the ground fibers has experienced a significant reduction of 50 % and 52 % for, respectively, 20 mm and 40 mm gage lengths. The stiffness of the pyrolyzed fibers with a gage length of 20 mm and 40mm, on the other hand, were 9 % and 17 % higher than those of the ground fibers, respectively. This observation is mainly attributed to the silica network compaction of the glass fibers, which results in higher density. In terms of the interfacial strength, the ground fibers showed an IFSS, 14 % and 26 % stronger than pyrolyzed and virgin glass fibers, respectively. Differences in the IFSS values result from the irregular lumps from epoxy residue on the surface of the ground fibers, a phenomenon which allows for molecular mechanical and chemical interactions. Using the IFSS and fibers strength values, a critical length rang of 0.57-1.14 mm and 0.54-0.78 mm were calculated for the ground and pyrolyzed fibers, respectively. These ranges can be used to design and analyze short recycled fibrous composites with effective mechanical properties.

Given this work has shown the relative merit of mechanically recycled fibers from scrap turbine blades over the pyrolyzed and virgin fibers, further experimental works are required to account for the effect of thermal and oxidative degradations on the IFSS. Due to inevitable variations in the resin residue on the surface of mechanically recycled fibers, future work on the exact macro-mechanical analysis of composites made of recycled fibers is proposed. The critical fiber length

values obtained in this study can be validated by manufacturing and testing polymer composites reinforced with recycled fibers.

Acknowledgments

A.R gratefully acknowledges Mr. Guangyu Bao and Biomechanics research laboratory for technical assistance with AFM. L.L and K.F acknowledge the funding provided by the Research Center for High Performance Polymer and Composite Systems (CREPEC), Project Vision; and The Natural Sciences and Engineering Research Council of Canada (NSERC), RGPIN- 2018-04144.

References

[1] Yang L, Thomason JL. Interface strength in glass fibre–polypropylene measured using the fibre pull-out and microbond methods. Composites Part A: Applied Science and Manufacturing. 2010;41(9):1077-83.

[2] Jang J, Yang H. Effect of surface treatment on the performance improvement of carbon fiber/polybenzoxazine composites. Journal of Materials Science. 2000;35:2297-303.

[3] Petersen HN, Kusano Y, Brøndsted P, Almdal K. Preliminary characterization of glass fiber sizing. Proceedings of the Risø International Symposium on Materials Science; 2013. p. 333-40.

[4] Cousins DS, Suzuki Y, Murray RE, Samaniuk JR, Stebner AP. Recycling glass fiber thermoplastic composites from wind turbine blades. Journal of Cleaner Production. 2019;209:1252-63.

[5] Larsen K. Recycling wind turbine blades. Renewable Energy Focus. 2009;9(7):70-3.

[6] Feih S, Manatpon K, Mathys Z, Gibson AG, Mouritz AP. Strength degradation of glass fibers at high temperatures. Journal of Materials Science. 2009;44(2):392-400.

[7] Ginder RS, Ozcan S. Recycling of Commercial E-glass Reinforced Thermoset Composites via Two Temperature Step Pyrolysis to Improve Recovered Fiber Tensile Strength and Failure Strain. Recycling. 2019;4(2):24.

[8] Nzioka AM, Kim YJ. Surface analysis of glass fibres using XPS and AFM: case study of glass fibres recovered from the glass fibre reinforced polymer using chemical recycling. Journal of Physics: Conference Series. 2018;953:012012.

[9] Cunliffe AM, Jones N, Williams PT. Pyrolysis of composite plastic waste. Environ Technol. 2003;24(5):653-63.

[10] Thomason J, Jenkins P, Yang L. Glass Fibre Strength—A Review with Relation to Composite Recycling. Fibers. 2016;4:18.

[11] Guo CC, Zhao Y, Chen D, Zhan MS. Effect of sizing agent on interfacial shear strength of carbon fibre composites. Materials Research Innovations. 2014;18(sup4):S4-997-S4-1002.

[12] Palmer J, Ghita O, Savage L, Evans K. Successful closed-loop recycling of thermoset composites. Composites Part A: Applied Science and Manufacturing. 2009;40(4):490-8.

[13] Chu J, Sullivan J. Recyclability of a continuous e-glass fiber reinforced polycarbonate composite. Polymer composites. 1996;17(4):556-67.

[14] Rahimizadeh A, Kalman J, Fayazbakhsh K, Lessard L. Recycling of fiberglass wind turbine blades into reinforced filaments for use in Additive Manufacturing. Composites Part B: Engineering. 2019;175:107101.

[15] Rahimizadeh A, Kalman J, Henri R, Fayazbakhsh K, Lessard L. Recycled Glass Fiber Composites from Wind Turbine Waste for 3D Printing Feedstock: Effects of Fiber Content and Interface on Mechanical Performance. Materials. 2019;12(23):3929.

[16] Shrivastava A. 4 - Additives for Plastics. In: Shrivastava A, editor. Introduction to Plastics Engineering: William Andrew Publishing; 2018. p. 111-41.

[17] Mallick PK. 13 - Testing the fatigue strength of fibers used in fiber-reinforced composites using fiber bundle tests. In: Guedes RM, editor. Creep and Fatigue in Polymer Matrix Composites: Woodhead Publishing; 2011. p. 409-23.

[18] Ibrahim I, Sarip S, Bani NA, Ibrahim MH, Hassan MZ. The Weibull probabilities analysis on the single kenaf fiber. AIP Conference Proceedings. 2018;1958(1):020009.

[19] Penn LS, Lee SM. Interpretation of the force trace for Kevlar/epoxy single filament pull-out tests. Fibre Science and Technology. 1982;17(2):91-7.

[20] Herrera-Franco PJ, Drzal LT. Comparison of methods for the measurement of fibre/matrix adhesion in composites. Composites. 1992;23(1):2-27.

[21] Burn DT, Harper LT, Johnson M, Warrior NA, Nagel U, Yang L, et al. The usability of recycled carbon fibres in short fibre thermoplastics: interfacial properties. Journal of Materials Science. 2016;51(16):7699-715.

[22] Cox HL. The elasticity and strength of paper and other fibrous materials. British Journal of Applied Physics. 1952;3(3):72-9.

[23] Mäder E, Freitag KH. Interface properties and their influence on short fibre composites. Composites. 1990;21(5):397-402.

[24] Choi N-S, Park J-E. Fiber/matrix interfacial shear strength measured by a quasi-disk microbond specimen. Composites Science and Technology. 2009;69(10):1615-22.

[25] Anane-Fenin K, Akinlabi E. Recycling of Fibre Reinforced Composites: A Review of Current Technologies: 4th International Conference on Development and Investment in Infrastructure - Strategies for Africa; 2017.

[26] Cunliffe AM, Jones N, Williams PT. Pyrolysis of composite plastic waste. Environmental Technology. 2003;24(5):653-63.

[27] Thomason JL, Kao CC, Ure J, Yang L. The strength of glass fibre reinforcement after exposure to elevated composite processing temperatures. Journal of Materials Science. 2014;49(1):153-62.

[28] Kennerley J, Kelly R, Fenwick N, Pickering S, Rudd C. The characterisation and reuse of glass fibres recycled from scrap composites by the action of a fluidised bed process. Composites Part A: Applied Science and Manufacturing. 1998;29(7):839-45.

[29] OTTO WH. Compaction Effects in Glass Fibers. Journal of the American Ceramic Society. 1961;44(2):68-72.

[30] Naik DL, Fronk TH. Weibull distribution analysis of the tensile strength of the kenaf bast fiber. Fibers and Polymers. 2016;17(10):1696-701.

[31] Ginder RS, Ozcan S. Recycling of Commercial E-glass Reinforced Thermoset Composites via Two Temperature Step Pyrolysis to Improve Recovered Fiber Tensile Strength and Failure Strain. Recycling. 2019:Medium: ED; Size: Article No. 24.

[32] Brydson JA. 26 - Epoxide Resins. In: Brydson JA, editor. Plastics Materials (Seventh Edition). Oxford: Butterworth-Heinemann; 1999. p. 744-77.

[33] Group SM. Recycling of waste glass fiber reinforced plastic with microwave pyrolysis (LIFE07 ENV/S/000904). Stena recycling, Göteborg, Sweden 2012.

[34] Bolduc S, Jung K, Venkata P, Ashokcline M, Jayasinghe R, Baillie C, et al. Banana fiber/low-density polyethylene recycled composites for third world eco-friendly construction applications – Waste for life project Sri Lanka. Journal of Reinforced Plastics and Composites. 2018;37(21):1322-31.

[35] Unterweger C, Brüggemann O, Fürst C. Effects of different fibers on the properties of short-fiber-reinforced polypropylene composites. Composites Science and Technology. 2014;103:49-55.

[36] Yang QS, Liu X. 13 - Mechanical behavior of extra-strong CNT fibers and their composites. In: Qin Q, Ye J, editors. Toughening Mechanisms in Composite Materials: Woodhead Publishing; 2015. p. 339-72.

[37] Liu BY, Wang XJ, Liu HY, Zhang G, Long SR, Yang J, et al. Effect of silane coupling agent and air plasma treatment on interfacial shear strength of carbon fiber/polyphenylene sulfide composites. In: Ye L, editor. Recent Advances in Structural Integrity Analysis - Proceedings of the International Congress (APCF/SIF-2014). Oxford: Woodhead Publishing; 2014. p. 365-9.

Figure captions and tables

Fig. 1 The recycling steps to reclaim fibers from scrap turbine blades: (A) scrap pieces from rotor blades; (B) ECO Wolf hammer mill grinder; (C) mechanically recycled ground fibers; (D) pyrolyzed ground fibers.

Fig. 2 Single fiber tensile test set-up.

Fig. 3 Procedure to prepare samples for single fiber pull-out test: (A) single fiber glued onto card tabs; (B) single PLA stripe is placed on a microscope slide and heated by a soldering iron; (C) the other end of the fiber is placed on the PLA stripe and heated again.

Fig. 4 The single fiber pull-out test sample: (A) specimen before the test; (B) specimen after the test.

Fig. 5 Linear interpolation to predict apparent IFSS.

Fig. 6 Diameter distribution of the recycled fibers.

Fig. 7 Morphology of glass fibers: (A) ground fibers; (B) pyrolyzed fibers; (C) virgin fibers.

Fig. 8 AFM height images showing the surface topology of fibers: (A) pyrolyzed fibers; (B) virgin fibers.

Fig. 9 Strength, stiffness and failure strain of recycled fibers: (A) ground fibers; (B) pyrolyzed fibers.

Fig. 10 Different types of defects present on the surface of ground fibers: (A) microscopic image from a long single ground fiber; (B) defects present on the surface of the ground fiber; (C) schematic showing the distribution of defects on the surface of a 20 mm and 40 mm ground fiber.

Fig. 11 Weibull function plot for single ground glass fibers with different gage lengths: (A) 20 mm; (B) 40 mm.

Fig. 12 Weibull function plot for single pyrolyzed glass fibers with different gage lengths: (A) 20 mm; (B) 40 mm; (C) 60 mm.

Fig. 13 Weibull function plot for single virgin glass fibers with different gage lengths: (A) 20 mm; (B) 40 mm; (C) 60 mm.

Fig. 14 Representative force-displacement curve and peak force vs. embedded length plots of single fiber pull out test for PLA and: (A) Pyrolyzed fibers; (B) ground glass fibers and (C) virgin glass fibers.

Table 1. The roughness results for the ground, pyrolyzed and virgin fibers.

	ground fibers			Pyrolyzed fibers			Virgin fibers		
	Right side	**Middle**	**Left side**	**Right side**	**Middle**	**Left side**	**Right side**	**Middle**	**Left side**
R_a (nm)	88.6	76.1	63.1	16.64	12.66	18.73	8.21	7.05	9.64
R_q (nm)	102.8	92.6	74.4	19.5	14.6	21.1	9.65	10	11.9

Table 2. Mechanical properties of the ground, pyrolyzed and virgin fibers.

Properties	**Mean strength (MPa)**			**Mean stiffness (GPa)**			**Mean strain to failure (%)**		
Gage length (mm)	20	40	60	20	40	60	20	40	60
Ground fibers	1990 ± 568	1678 ± 580	876 ± 377*	76 ± 13	74 ± 12	74 ± 11*	2.32 ± 0.6	2.1 ± 0.7	1.1 ± 0.5*
Pyrolyzed fibers	976 ± 260	806 ± 217	679 ± 122	84 ± 12	89 ± 10	91 ± 22	1.23 ± 0.3	0.93 ± 0.17	0.77 ± 0.13
Virgin fibers	2485 ± 508	2073 ± 251	1965 ± 353	71 ± 7	74 ± 9	77 ± 8	3.5 ± 0.6	2.8 ± 0.3	2.7 ± 0.5

*The asterisk symbol shows the results that were obtained with lower number of samples

Table 3. The Weibull parameters for the ground, pyrolyzed and virgin fibers with different gage lengths.

	Ground fibers		**Pyrolyzed fibers**			**Virgin fibers**		
Gage length (mm)	20	40	20	40	60	20	40	60
Scale parameter (σ_0)	2190	1892	1073	904	729	2700	2178	2106
Shape parameter (w)	4.22	2.94	4.25	3.78	6.27	5.8	9.87	6.6

Table 4. The value of IFSS and critical length for the ground and pyrolyzed fibers.

Fiber type	**τ_{d1} (MPa)**	**R^2**	**Critical length, lower bound l_c (mm)**	**Critical Length, upper bound l_c (mm)**
Virgin fibers	9.54	0.57		
Ground fibers	13.01	0.75	0.57	1.14
Pyrolyzed fibers	11.23	0.51	0.54	0.78

Figures

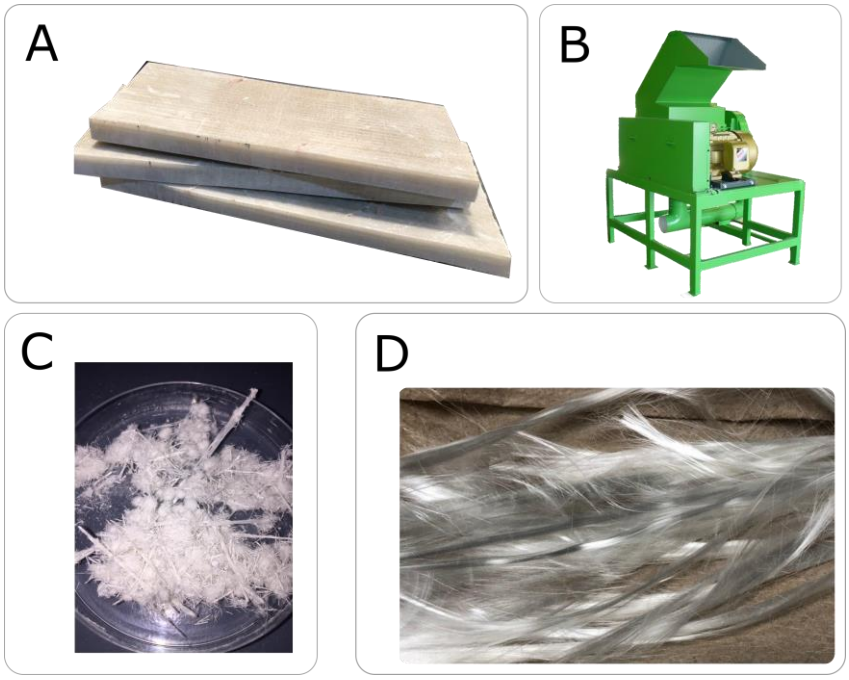

Fig 1. The recycling steps to reclaim fibers from scrap turbine blades: (A) Scrap pieces from rotor blades; (B) ECO Wolf hammer mill grinder; (C) mechanically recycled ground fibers; (D) pyrolyzed ground fibers.

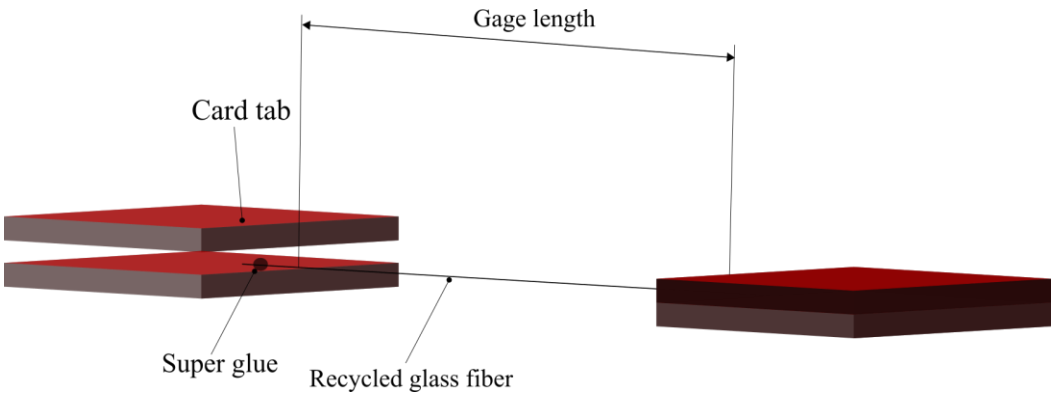

Fig 2. Single fiber tensile test set-up.

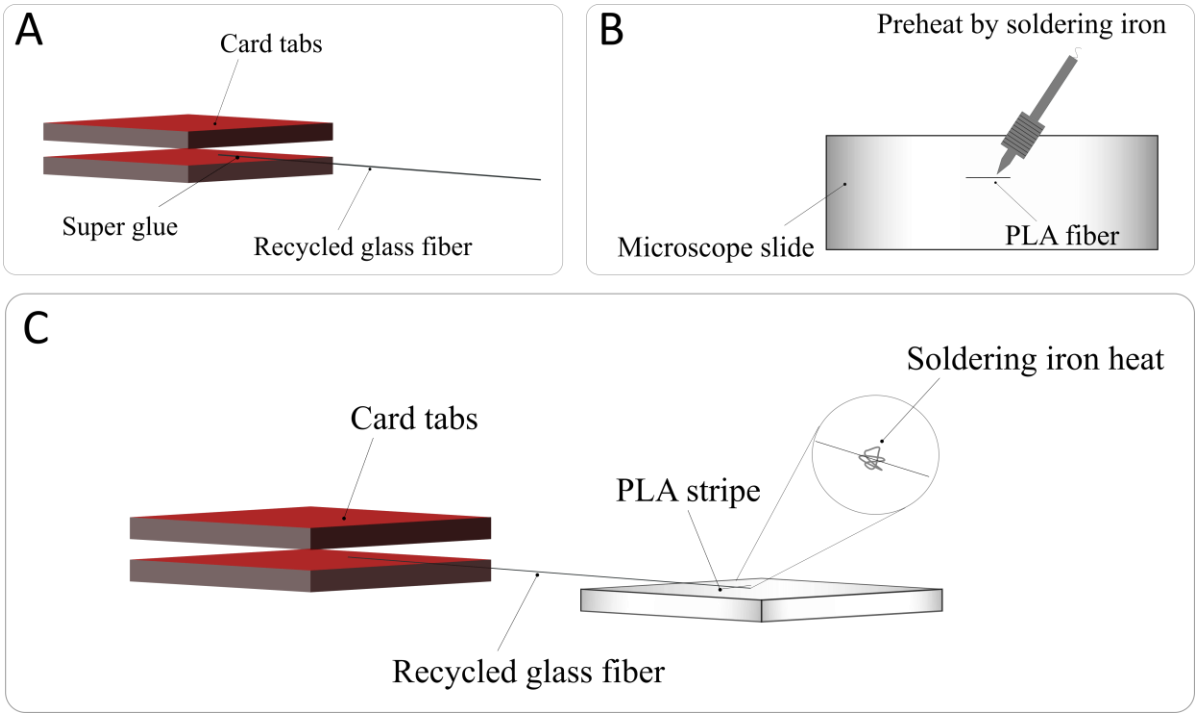

Fig 3. Procedure to prepare samples for single fiber pull-out test: (A) single fiber glued onto card tabs; (B) single PLA stripe is placed on a microscope slide and heated by a soldering iron; (C) the other end of the fiber is placed on the PLA stripe and heated again.

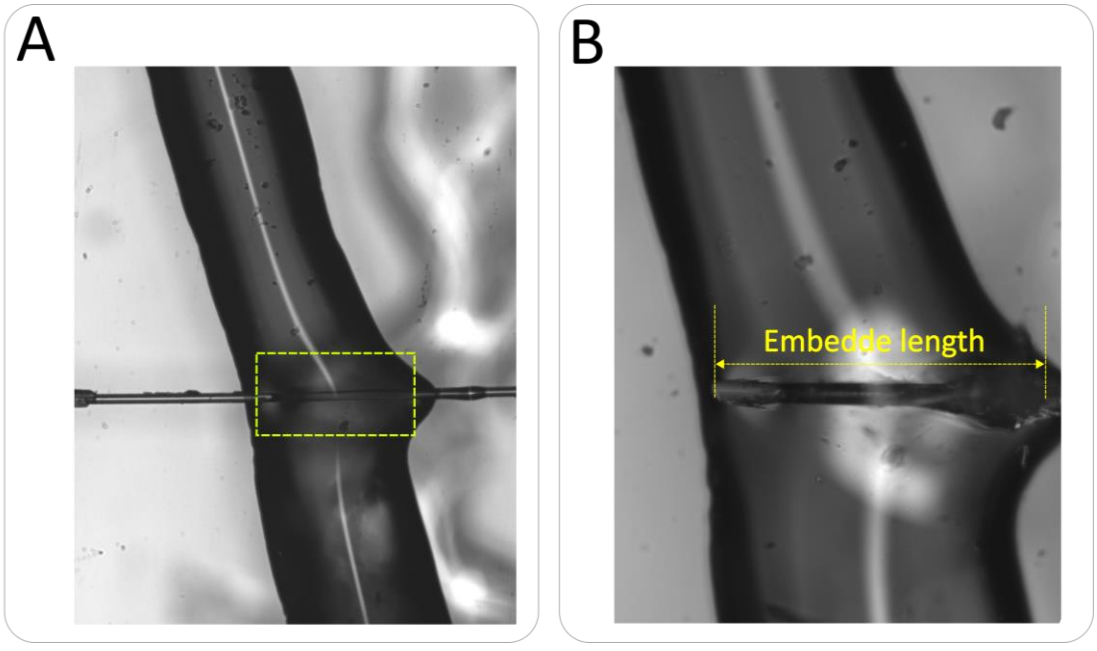

Fig 4. The single fiber pull-out test sample: (A) specimen before the test; (B) specimen after the test.

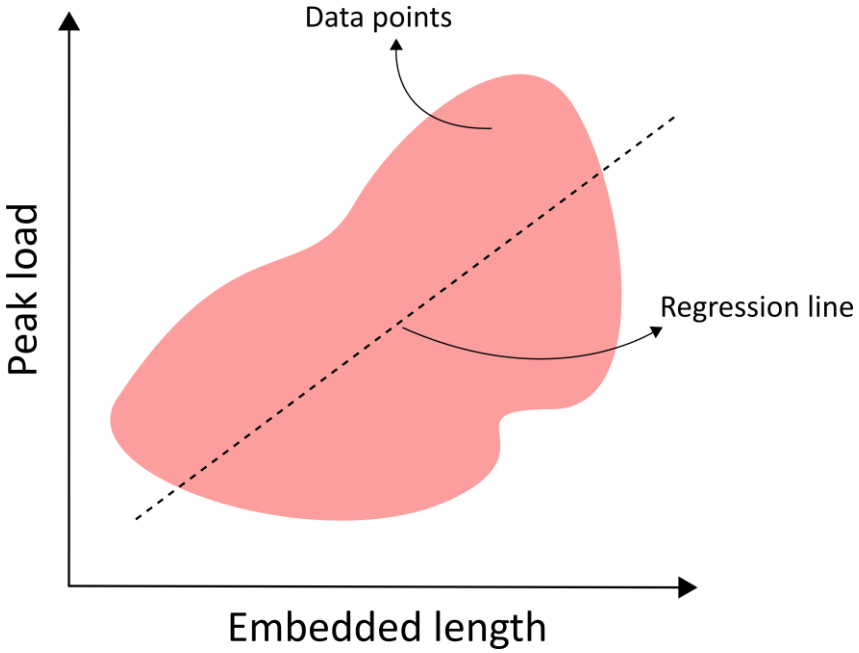

Fig 5. Linear interpolation to predict apparent IFSS.

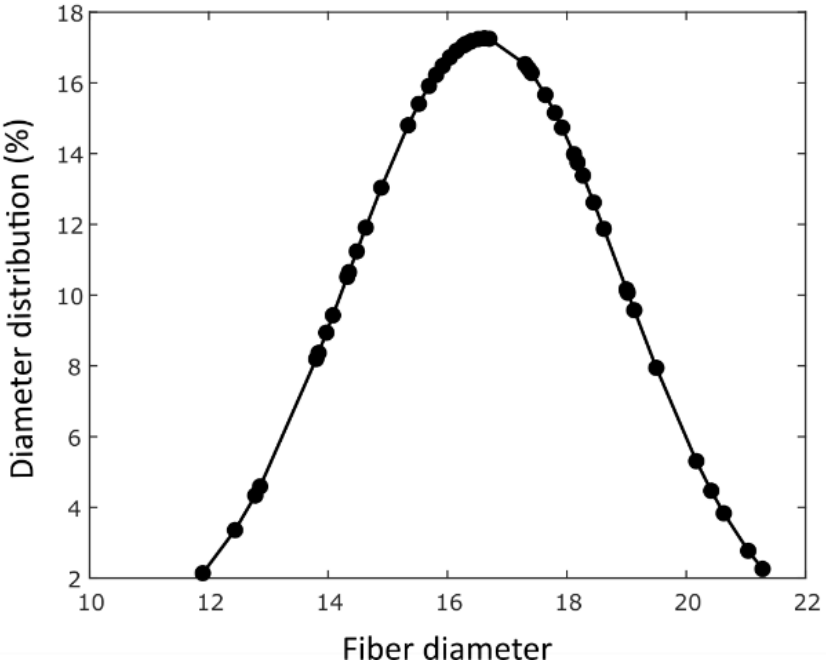

Fig 6. Diameter distribution of the recycled fibers.

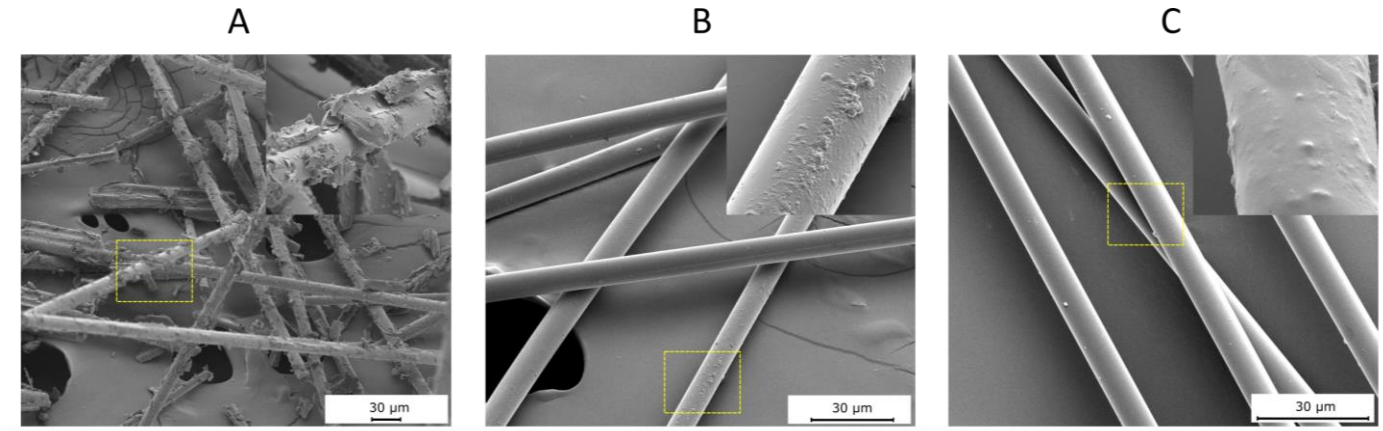

Fig 7. Surface morphology of the fibers: (A) ground fibers; (B) pyrolyzed fibers; (C) virgin fibers.

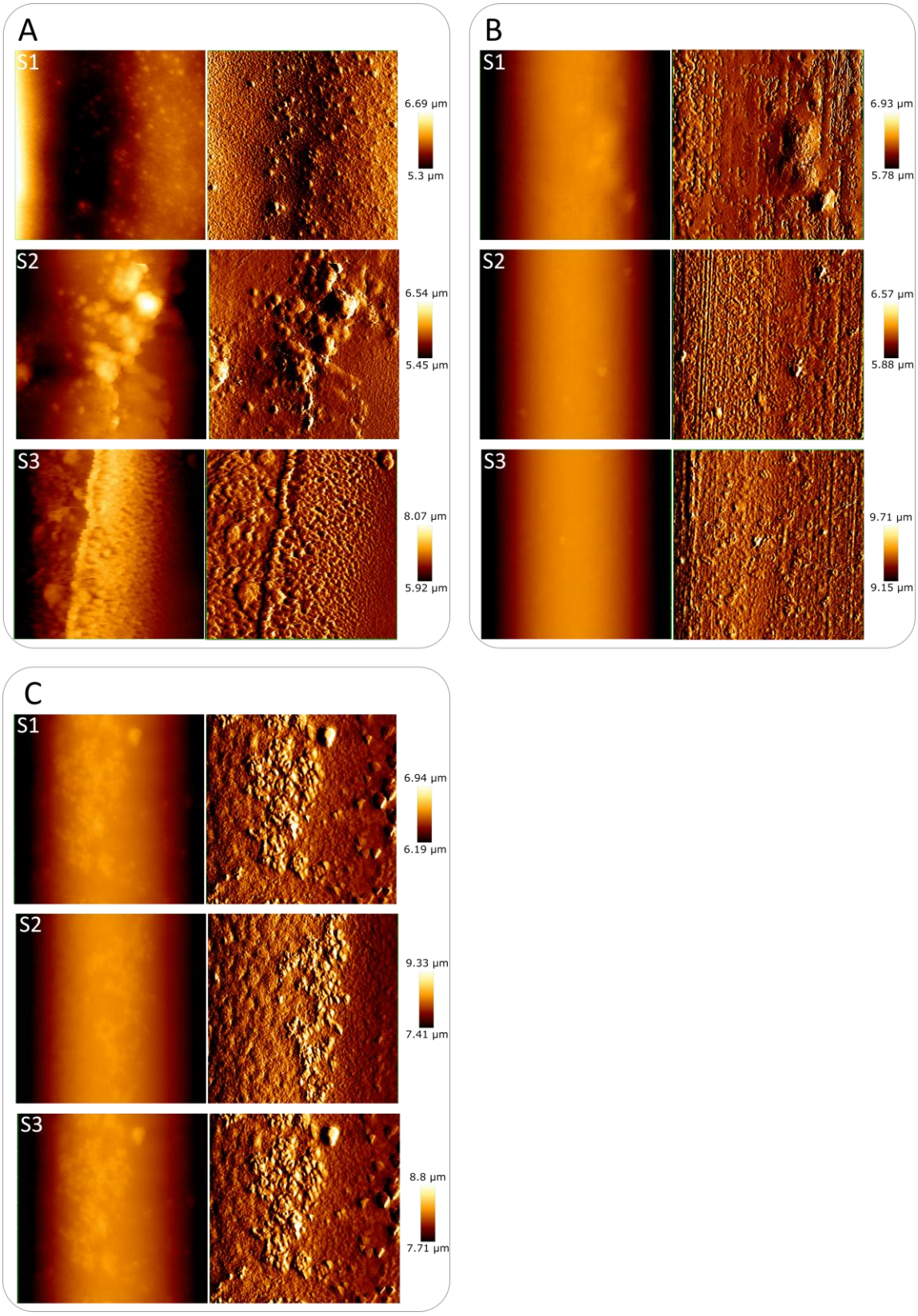

Fig 8. AFM height images showing the surface topology of the fibers: (A) ground fibers; (B) pyrolyzed fibers; (C) virgin fibers.

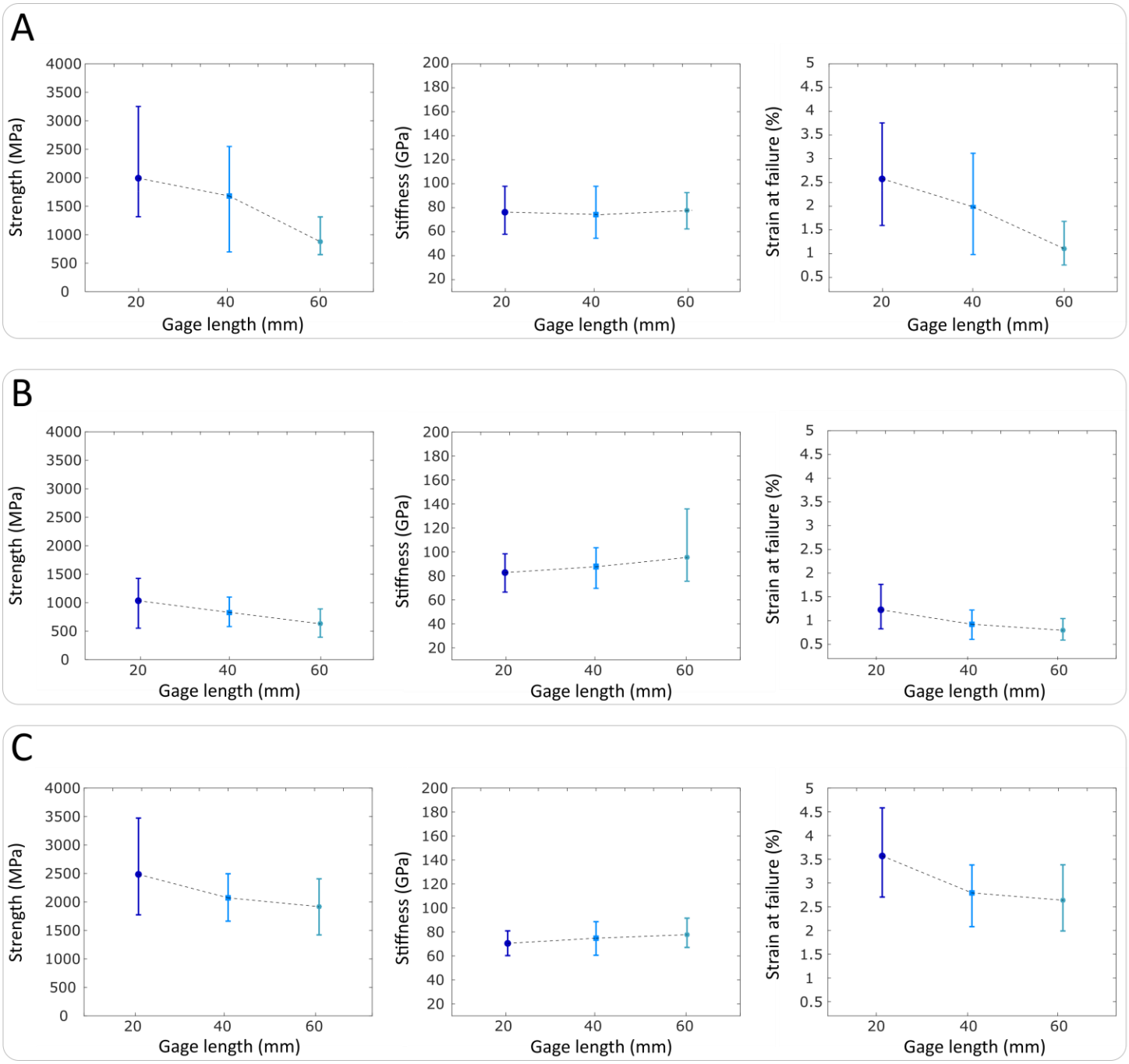

Fig 9. Strength, stiffness and failure strain of the fibers: (A) ground fibers; (B) pyrolyzed fibers; (C) virgin fibers.

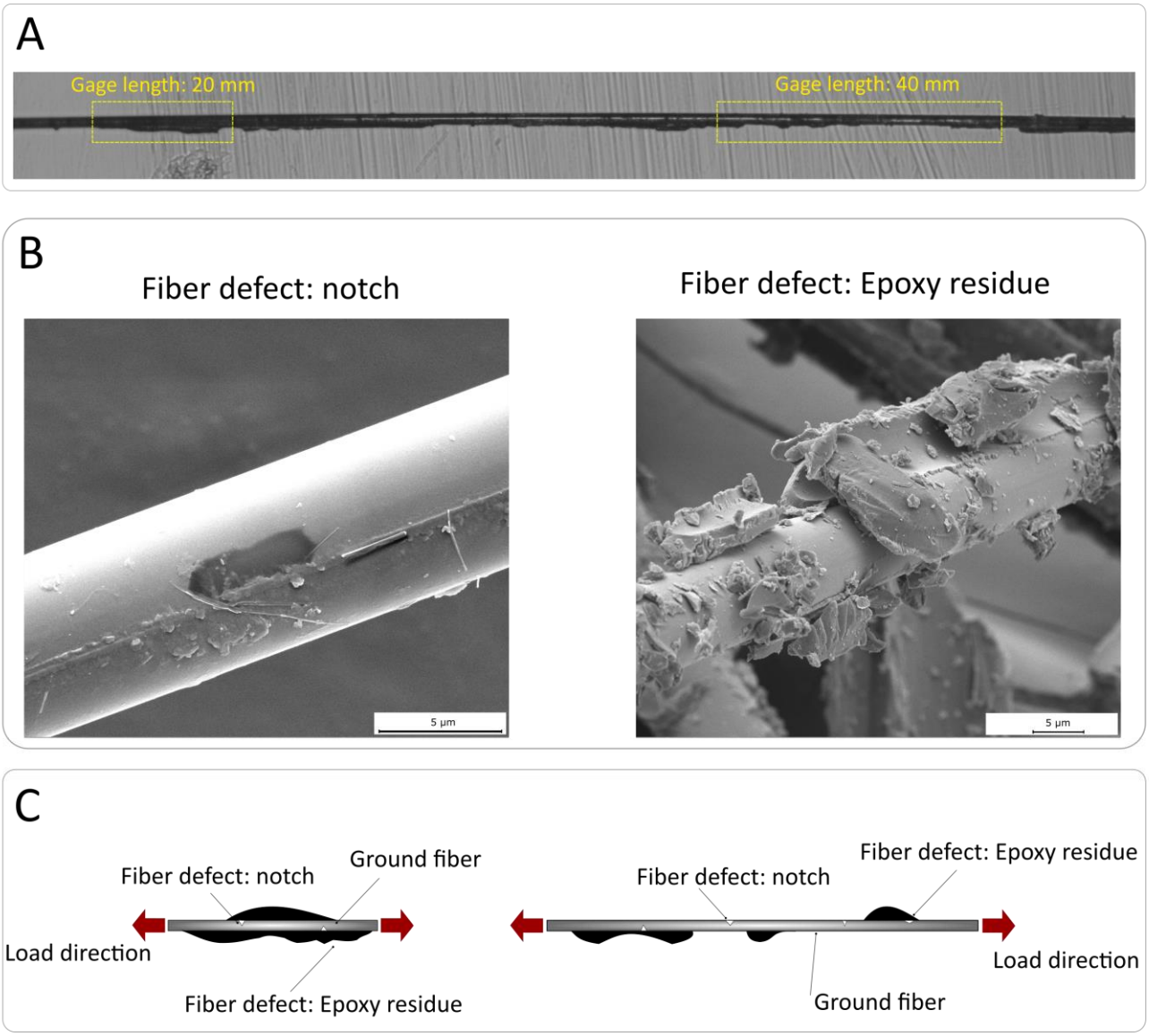

Fig 10. Different types of defects present on the surface of ground fibers: (A) microscopic image from a long single ground fiber; (B) defects present on the surface of the ground fiber; (C) schematic showing the distribution of defects on the surface of a 20 mm and 40 mm ground fiber.

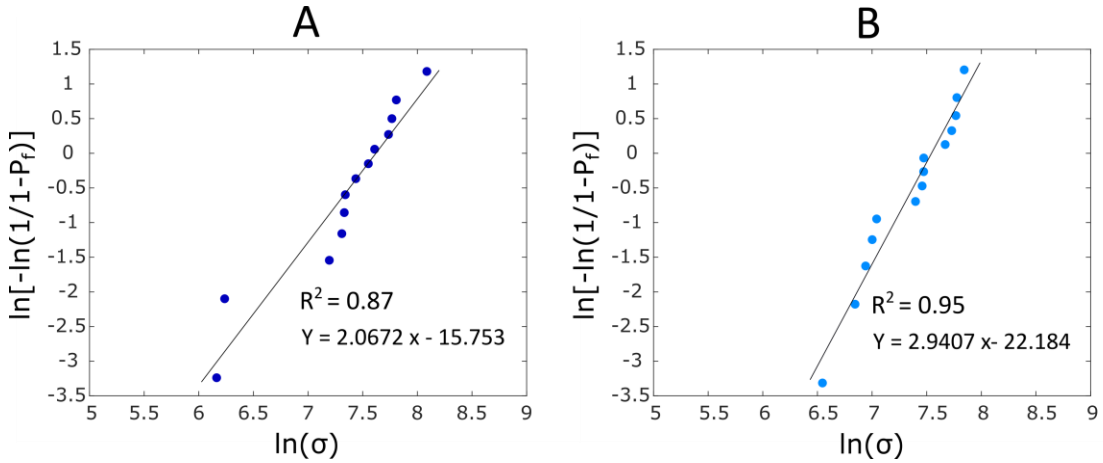

Fig 11. Weibull function plot for single ground glass fibers with different gage lengths: (A) 20 mm; (B) 40 mm.

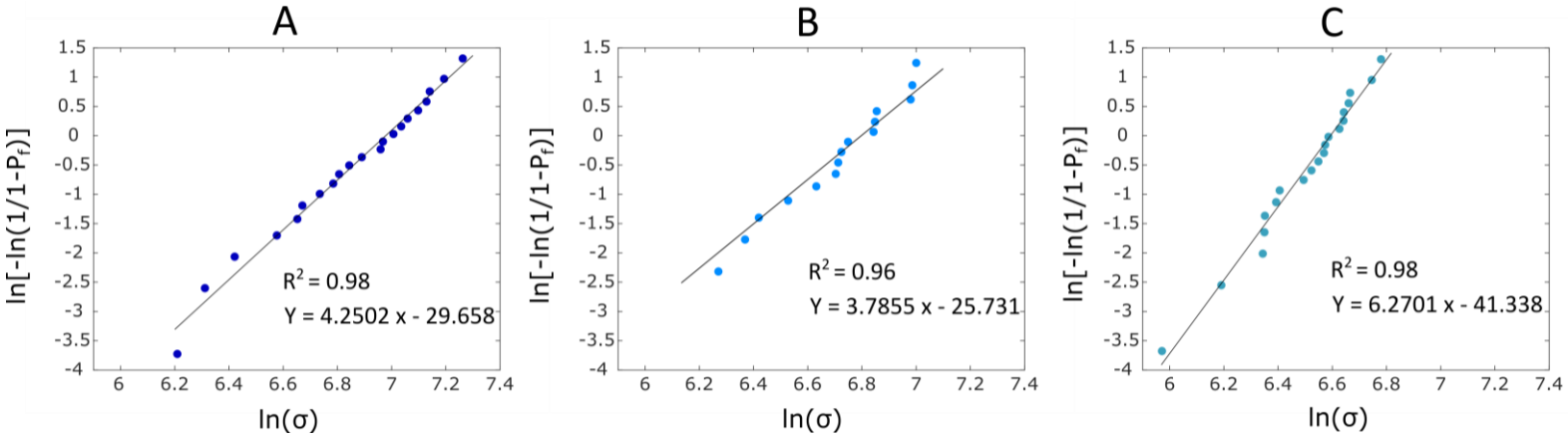

Fig 12. Weibull function plot for single pyrolyzed glass fibers with different gage lengths: (A) 20 mm; (B) 40 mm; (C) 60 mm.

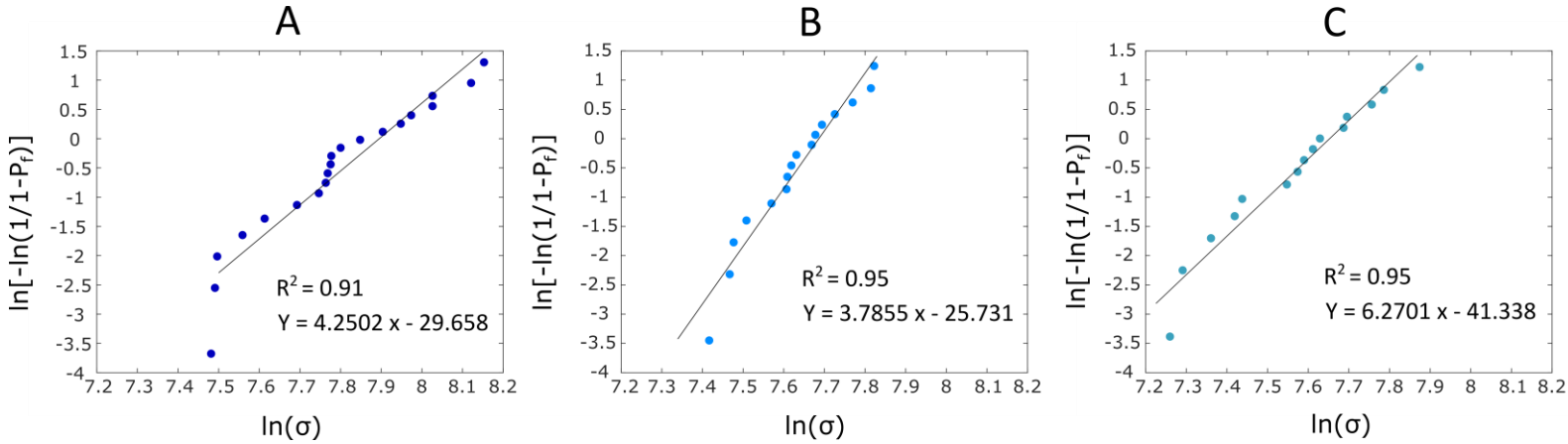

Fig 13. Weibull function plot for single virgin glass fibers with different gage lengths: (A) 20 mm; (B) 40 mm; (C) 60 mm.

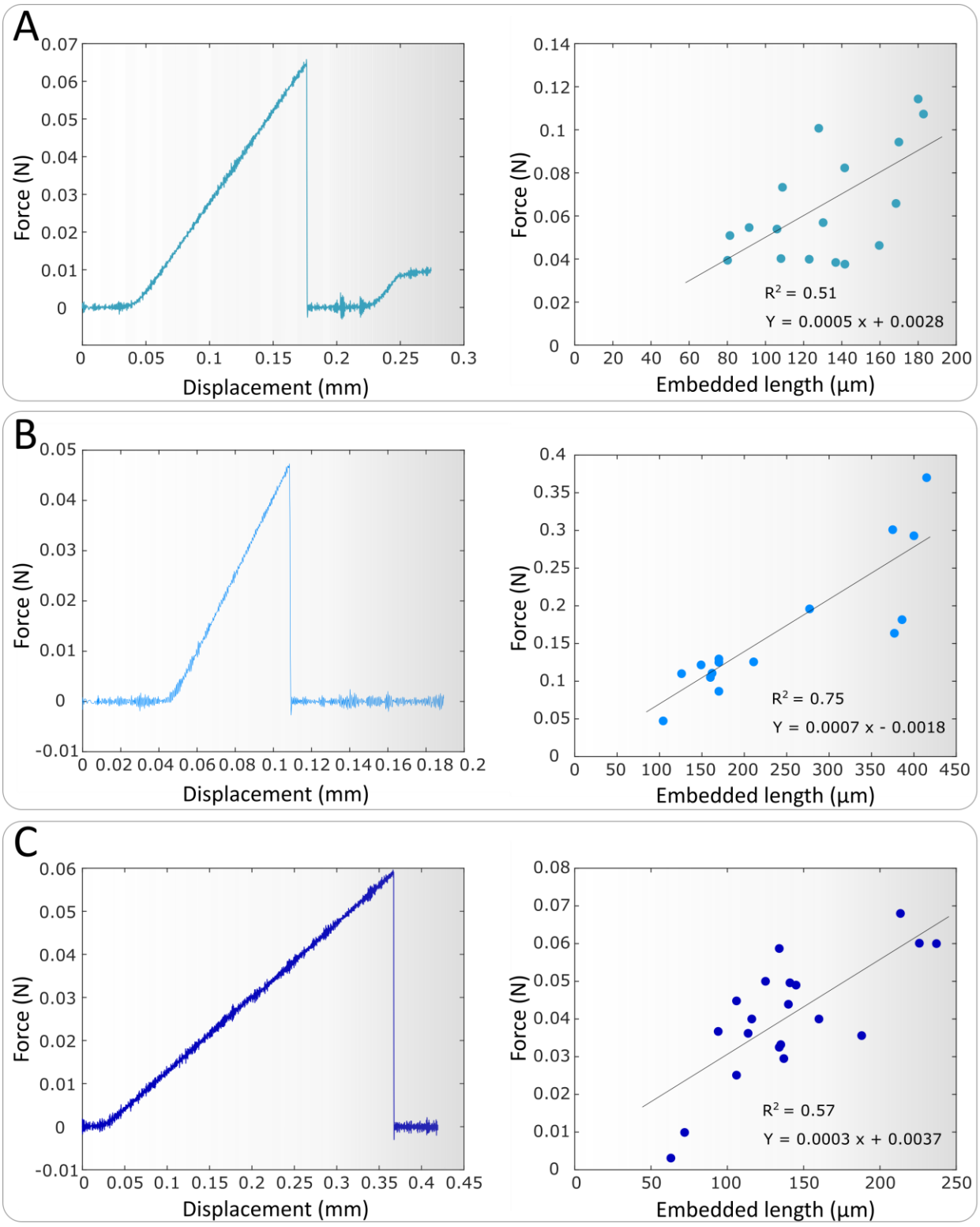

Fig 14. Representative force-displacement curve and peak force vs. embedded length plots of single fiber pull out test for PLA and: (A) Pyrolyzed fibers; (B) ground fibers and (C) virgin fibers.